Title
Insights Into Pulp Biomineralization in Human Teeth

Authors
He, Rui
Chou, Conrad
Chen, Ling
et al.

Publication Date
2023-07-10

DOI
10.3389/fdmed.2022.883336

Peer reviewed

frontiers | Frontiers in Dental Medicine

ORIGINAL RESEARCH
published: 03 May 2022
doi: 10.3389/fdmed.2022.883336

Insights Into Pulp Biomineralization in Human Teeth

Rui He[1,2], *Conrad Chou*[3], *Ling Chen*[1], *Marshall Stoller*[4], *Misun Kang*[1] *and Sunita P. Ho*[1,4]*

[1] Division of Preclinical Education, Biomaterials and Engineering, Department of Preventive and Restorative Dental Sciences, School of Dentistry, University of California, San Francisco, San Francisco, CA, United States, [2] Hangzhou Normal University, Hangzhou, China, [3] Division of Pediatric Dentistry, Department of Oral and Craniofacial Sciences, School of Dentistry, University of California, San Francisco, San Francisco, CA, United States, [4] Department of Urology, School of Medicine, University of California, San Francisco, San Francisco, CA, United States

Introduction: Mineralized pulp (MP) compromises tooth function and its causation is unknown. The hypothesis of this study is that pulp mineralization is associated with pulpal tissue adaptation, increased mineral densities, and decreased permeabilities of tubular dentin and cementum. Methods will include correlative spatial mapping of physicochemical and biochemical characteristics of pulp, and contextualize these properties within the dentin-pulp complex (DPC) to reveal the inherent vunerabilities of pulp.

Methods: Specimens ($N = 25$) were scanned using micro X-ray computed tomography (micro-XCT) to visualize MP and measure mineral density (MD). Elemental spatial maps of MP were acquired using synchrotron X-ray fluorescence microprobe (μXRF) and energy dispersive X-ray spectroscopy (EDX). Extracted pulp tissues were sectioned for immunolabelling and the sections were imaged using a light microscope. Microscale morphologies and nanoscale ultrastructures of MP were imaged using scanning electron (SEM) and scanning transmission electron microscopy (STEM) techniques.

Results: Heterogeneous distribution of MD from 200 to 2,200 mg/cc, and an average MD of 892 (±407) mg/cc were observed. Highly mineralized pulp with increased number of occluded tubules, reduced pore diameter in cementum, and decreased connectivity in lateral channels were observed. H&E, trichrome, and von Kossa staining showed lower cell and collagen densities, and mineralized regions in pulp. The biomolecules osteopontin (OPN), osteocalcin (OCN), osterix (OSX), and bone sialoprotein (BSP) were immunolocalized around PGP 9.5 positive neurovascular bundles in MP. SEM and STEM revealed a wide range of nano/micro particulates in dentin tubules and spherulitic mineral aggregates in the collagen with intrafibrillar mineral surrounding neurovascular bundles. EDX and μXRF showed elevated counts of Ca, P, Mg, and Zn inside pulp and at the dentin-pulp interface (DPI) in the DPC.

Conclusion: Colocalization of physical and chemical, and biomolecular compositions in MP suggest primary and secondary biomineralization pathways in pulp and

OPEN ACCESS

Edited by:
Brian L. Foster,
The Ohio State University,
United States

Reviewed by:
Sarah Peters,
The Ohio State University,
United States
Monica Prasad Gibson,
University of Alberta, Canada

***Correspondence:**
Sunita P. Ho
sunita.ho@ucsf.edu

Specialty section:
This article was submitted to Systems Integration, a section of the journal Frontiers in Dental Medicine

Received: *24 February 2022*
Accepted: *09 March 2022*
Published: *03 May 2022*

Citation:
He R, Chou C, Chen L, Stoller M, Kang M and Ho SP (2022) Insights Into Pulp Biomineralization in Human Teeth. Front. Dent. Med. 3:883336. doi: 10.3389/fdmed.2022.883336

dentin at a tissue level, and altered fluid dynamics at an organ level. Elevated counts of Zn at the mineralizing front in MP indicated its role in pulp biomineralization. These observations underpin the inherent mechano- and chemo-responsiveness of the neurovascular DPC and help elucidate the clinical subtleties related to pulpitis, dentin-bridge, and pulp stone formation.

Keywords: pulp biomineralization, pulp, interstitial fluid pressure, dentin-pulp complex, permeability

INTRODUCTION

Dental pulp is a cellular organic network of blood and lymphatic vessels interspersed with nerves. This neurovascular organic network is housed in a spacious tooth-chamber and the relatively narrowed root-canal spaces of a tooth. The vascularized and innervated pulp provides nutrients to cells within tissues of teeth. The pulp is compartmentalized into several zones with varying densities of cells, blood vessels, and nerves (1). This multi-zonal organ from a bioengineering perspective exhibits a relatively higher hydrostatic pressure compared to other organs, contains regenerative cells, and is encapsulated within the harder yet permeable walls of the predominantly inorganic dentin. The natural "control systems" that maintain the interstitial fluid pressure (IFP) of the pulp include lymphatic vessels and capillaries (2–4). These control systems regulate interstitial fluid flow from the pulp through the dentin tubules to the enamel coronally, and to cementum apically (1). They maintain local concentrations of plasma proteins within the zones, and the overall osmotic pressure within pulp. The higher IFP prevents bacterial invasion and maintains overall functional homeostasis not limited to pulp, but also the dentin-pulp complex (DPC) (2, 5–7). Mineralization of this functionally influential pulpal organ has been phrased as pulp mineralization (1) with minimal to no information on its causation. Clinically, it commonly manifests as pulp stone, and dentin-bridge formation (8–10).

Biominerals within pulp to date have undergone rudimentary investigations, despite being identified and categorized as free or embedded in pulp, and/or attached to dentin (11). Mineralization of the innervated and vascularized pulp can result from sterile or non-sterile inflammation (12), and from pathways similar to those reported in neurovascular skeletal and smooth muscles (13). The primary effectors that inextricably shift the IFP of the vascularized and innervated pressurized pulp include molecular- and tissue-level factors that occur locally at site-specific anatomical locations. These factors include: (1) changes in permeabilities and mineral densities of dentin and cementum that affect fluid transport between pulp and the periodontal complex (5, 14, 15), and (2) inflammation-induced vasodilation and swelling (2). Secondary effectors that can potentiate the aforementioned primary effectors at the level of a DPC include: (3) anatomy-specific tooth architecture, in particular, the apical orifice "strangulation" of an already inflamed pulp (4); and consequently (4) ischemia related altered oxygen supply to the local regions of the pulp (4).

The physiologically beneficial characteristic of higher IFP, ironically can increase beyond normal limit when the tooth is insulted (orthodontic forces, pulpitis, trauma, auto-transplantation) (16). This net increase in IFP invariably "tips" the homeostatic balance and triggers acute or chronic inflammatory pathway(s). The impact of the inflammatory pathways on the pulp also depends on the magnitude, frequency and duration of the insult, and masticatory function (1, 5, 12, 14). Conceivably, this naturally engineered pressure chamber is mechanically stressed and strained, and contains pressure and chemical graidents. These gradients are encouraged by balanced concentrations of biomolecules and ions across the many zones and tissue interfaces including the dentin-pulp and -cementum interfaces.

Interfaces across the many disparate tissues of a tooth are a part and parcel of the intricate interconnected network that can affect fluid flow between pulp and the periodontal complex. The impaired cementum, dentin or pulp, as such, can alter the homeostasis of pulp at multiple length scales, which will be the topic of discussion, but within the framework of pulp biomineralization. The hypothesis of this study is that pulp mineralization is associated with pulpal tissue adaptation, and increased mineral densities and decreased permeabilities of tubular dentin and cementum. Study outcomes will confirm that the mineralized pulp in non-carious human permanent teeth is associated with altered constituents of the pulp, and compromised physicochemical characteristics of tubular dentin and cementum. Methods will include correlative spatial mapping of physicochemical and biochemical characteristics of pulp, and contextualize these properties within the DPC to reveal the inherent vunerabilities of pulp. This multiscale correlative approach will provide insights into the plausible predisposed nature of tissues (17–21), and in this case pulp, that can form biominerals as a response to significant shifts in the IFP. From a practical standpoint, it will reveal the need to question the effect of clinical interventions such as local anesthesia (22), dental restorations (23), periodontal treatment (24), and orthodontics (16), all of which can significantly affect functional homeostasis of the pulp.

MATERIALS AND METHODS

As mentioned, a multiscale correlative microspectroscopic approach (17–21) was taken to gather insights into pulp biomineralization. Methods include a length-scale mapping of physical, chemical, and biochemical characteristics of pulp,

dentin, and cementum. Post analyses of the acquired data within the context of the DPC will reveal insights into plausible biomineralization pathways of pulp in non-carious human teeth.

Specimen Preparation

Fresh human non-carious permanent teeth that were extracted (including both anterior and posterior) for orthodontic, periodontic, and prosthodontic reasons were used in this study. These undocumented (with no identifiers including age and gender of the patient) teeth were prepared within the guidelines of Human Research Protection Program Institutional Review Board of UCSF (Study Number: 16-19606). Teeth ($N = 25$) were fixed in 10% neutral buffered formalin (NBF, Richard-Allan Scientific, Kalamazoo, MI, USA) overnight at 4°C, washed three times in 1x phosphate buffered saline (PBS), and were stored in 70% ethanol solution at 4°C.

Light Microscopy and Micro X-Ray Computed Tomography

Image Acquisition

The root canals of the specimens were scanned in 70% ethanol using micro X-ray computed tomography (micro-XCT) system (MicroXCT-200, Carl Zeiss Microscopy, Pleasanton, CA) at 2X (9 μm/voxel) and 4X (5 μm/voxel) magnification with 80 kVp (2X) and 50 kVp (4X) of voltage and 8 W of power. X-ray tomograms (virtual slices) were reconstructed using XM Reconstructor following center offset and beam hardening corrections (25).

Specimens were sectioned into two halves along the longitudinal axis with a slow-speed diamond saw (Isomet, Buehler, Lake Bluff, IL) following X-ray scanning. Reflection and transmission optical images of the sectioned halves were acquired using a light microscope (LM) (SZ61, Olympus, Tokyo, Japan). The extracted pulp from each tooth was imaged using micro-XCT, and the specimens were further processed for immunohistochemistry and subsequently for correlative microspectroscopy. Pulp without detectable minerals by X-rays served as controls.

Image Analyses

The reconstructed images of the root canals with intact pulp, and pulp isolated from teeth were analyzed using AVIZO 2019.2 software (Fisher Scientific, Hillsboro, OR). X-ray intensity values were converted to mineral densities (MD, mg/cc) following a published calibration protocol (25). Mineralized regions were segmented, and histograms illustrating the frequency of MD occurrences were plotted. A Gaussian curve was fitted to the average MD histogram obtained from all scanned specimens using a curve fitting tool in MATLAB (19). The lateral channels and pores in cementum specific to the roots were segmented, and the pore diameter distribution within cementum volumes were obtained. Regions of interest from the root canal through dentin were selected, and MD profiles across the root (root diameter) were mapped using Fiji.

Field Emission Scanning Electron Microscopy and Scanning Transmission Electron Microscopy

The sectioned specimens were dehydrated using ascending series of ethanol solutions (from 50 to 100%) for field emission scanning electron microscopy (SEM, SIGMA VP500, Carl Zeiss Microscopy, Pleasanton, CA). Surface morphologies of dentin and pulp were imaged at 1 keV. Specimens were infiltrated with LR-white resin (Electron Microscopy Sciences, Hatfield, PA) in a gelatin capsule and polymerized for 2 days at 60°C and cut into 90 nm thin ultrasections with an ultramicrotome (Reichert Ultracut E, Leica Microsystems, Inc., Buffalo Grove, IL). The ultrasections were collected on formvar/carbon-coated Ni grids (Electron Microscopy Sciences) and were imaged for ultrastructure using scanning transmission electron microscopy (STEM, SIGMA VP500, Carl Zeiss Microscopy, Pleasanton, CA) mode at 15 keV (17, 18).

Histology, Immunohistochemistry, and Immunofluorescence

Extracted yet intact pulp (undemineralized) was processed using 15 and 30% sucrose solutions, embedded in optimal cutting temperature (OCT) medium, and cryosectioned to make 6–7 μm thick transverse sections. Sections from all specimens were stained with hematoxylin and eosin (H&E), Masson's trichrome (MT), and von Kossa to localize cell nuclei, collagen, and calcified regions (17), respectively.

For immunohistochemistry (IHC), epitope retrieval was achieved with 0.1 M sodium citrate buffer (pH = 6.0) for 30 min at 80°C for all sections. Sections were then blocked for endogenous peroxidases by immersion in 0.6% hydrogen peroxide in 80% methanol for 30 min at 25°C. Blocking of all sections was performed with the addition of 20% normal goat serum and 2.5% bovine serum albumin (Sigma-Aldrich) in PBS solution for 60 min at 25°C just prior to the addition of primary antibody. Sections were incubated overnight at 4°C with anti-PGP 9.5 (1:500 rabbit monoclonal antibody, AB108986; Abcam) for nerves (26), and for acidic molecule location anti-OPN (1:200 mouse monoclonal antibody, sc-73631, Santa Cruz Biotechnology Inc., Dallas, TX), anti-OCN (1:200 mouse monoclonal antibody, sc-73464, Santa Cruz Biotechnology Inc., Dallas, TX), and anti-BSP (1:200 mouse monoclonal antibody, sc-73630, Santa Cruz Biotechnology, Inc, Dallas, TX) were used. Anti-OSX (1:200 mouse monoclonal antibody, sc-393325; Santa Cruz Biotechnology, Inc, Dallas, TX), an osteogenic transcription factor was spatially localized using immunofluorescence microscopy. The staining reactions of secondary antibody DAB from Vector Lab (Burlingame, CA) and Alexa Fluor Donkey anti-rat IgG AF568 secondary antibody (AB175475; Abcam) at a 1:200 dilution were performed following the protocols provided in the kits. Hoechst 33342 solution (5 μg/ml) was utilized as counterstain for IF. After counterstaining, all sections were dehydrated and sealed using DPX mount (Sigma-Aldrich, St. Louis, MO). All experimental staining procedures were accompanied by control slides replacing primary antibody binding with blocking solution

containing 5% normal goat serum and 2.5% BSA in PBS to assess the level of non-specific staining. Slides were examined at 40X (water objective) using a light microscope with various fluorescence filters (Zeiss Observer Z1, Axiocam 506) (26).

Correlative Light and Electron Microscopy of Histology Sections

The matrix structure was examined at a higher resolution and was correlated with histologic stains, and immunolocalized biomolecules. Following light microscopy of stained and immunolocalized tissues, sections were further examined at a higher resolution by collecting the field emission electrons using FESEM at a scanning electron voltage of 1keV (17, 21).

Energy Dispersive X-Ray, and Microprobe X-Ray Fluorescence Spectroscopy

The chemical composition of intact pulp was acquired using an energy dispersive X-ray detector (EDX, Bruker AXS, Madison, WI) at 15 keV. Phase analysis was performed using cluster method in Esprit 2 software (Bruker Nano Inc., Madison, Wis., US). Elemental maps specific to zinc (Zn) and magnesium (Mg) in addition to commonly identified calcium (Ca) and phosphorus (P) of roots and pulp from teeth also were collected using the X-ray fluorescence microprobe (μ-XRF) at beamline 10.3.2 of Advanced Light Source (ALS) at Lawrence Berkeley National Laboratory (LBNL). Spatial maps of elemental counts were generated using an incident energy beam of 10 keV and a spot size of $\sim 8 \times 8\,\mu m$ (17, 19).

RESULTS

Results will illustrate that the structural and mineral density changes in tubular dentin and cementum within human molars are associated with mineralizing neurovascular organic network. At a microscale tissue-level, data will illustrate that the mineralizing pulp is contained within tubular dentin occluded with various Zn and Mg containing mineralized nanoparticles, and microscale aggregates of the same spread into larger volumes of the organic network. Furthermore, at a macroscale tooth-level, data will illustrate that pulp mineralization is associated with decreased cementum permeability and increased accessory (lateral) channel occlusion.

Mineral Densities of Mineralized Pulp

Mineralized pulp and adapted dentin regardless of tooth type (anterior, premolar, and molar) were observed using reflection and transmission light microscopy (LM) (**Figure 1A**) modes. Regions of adapted dentin were observed by capturing scattered and attenuated light (dashed outlined white and dark regions, **Figure 1A**), respectively. Reconstructed digital volumes of pulp extracted from teeth using CT data illustrated a distribution of lower and higher mineralized regions (**Figure 1B**) along the root. Lower and higher MDs also were observed in the transverse sections (asterisks *-***, **Figure 1B**), and this pattern was consistent across all tooth types (**Figure 1C**). The MD range of mineralized pulp was ∼200–2,200 mg/cc (**Figure 1C**) and on average was 892 ± 407 mg/cc; pulp MD is lower than most hard tissues (**Figure 1D**). However, on occasion, the highest MD (molar in **Figure 1**, MD: 1,757 ± 361 mg/cc) of mineralized pulp was greater than that of human dentin (1,540 ± 5 mg/cc).

Root Canal, Radicular Mineralized Pulp, Cementum Pore Distribution, and Accessory Channels in Roots

The root canal (RC, blue), mineralized pulp (MP, white), accessory channels, and pores (red) in cementum with three transverse sections (top, middle, bottom) from three different teeth are shown (**Figures 2A–C**). These digitally reconstructed volumes illustrated more lateral channels and cementum pores in teeth with less mineralized pulp (a, first column). Higher mineral density regions (dotted circle, **D**) adjacent to the root canal were observed from the root canal through dentin into cementum (**Figure 2D**). The mineral density distributions and cementum thicknesses were different between roots (**Figure 2D**). Volumes of mineralized pulp and cementum pore diameters are summarized in table (**Figure 2E**). Roots with less mineralized pulp contained cementum pores of larger diameters [box plots with higher standard variation (**Figure 2F**)]. Occluded tubules with nano/micro particles (red arrowhead) inside dentin tubules adjacent to pulp, and thickening of peritubular dentin also resulting in narrowing of lumen in the dentin (**Figure 2G**) were observed. See **Supplementary Movie S1**.

Immunolocalization of Neurovascular Bundles and Osteogenic Proteins in Mineralized Pulp

Higher mineral density at the DPI, and relatively lower mineral density away from the DPI were observed in representative transverse X-ray tomogram (**Figures 3A**,a). Lower cell densities (H&E, b) and blood vessels within collagenous matrix (MT, c) were surrounded by mineralized regions (von Kossa, **Figures 3A**,d). Odontoblasts, odontoblasts processes, and dentin tubules (red rectangle in b illustrates) in physical association with the DPC [red arrowhead in X-ray and light micrographs, (**Figure 3A**)] were observed. Acidic proteins, OCN, and OPN were localized around vasculature (**Figures 3A**,e,f). Localization of anti-protein gene product (PGP) 9.5 (**Figures 3A**,g) and α-SMA (**Figures 3A**,h) illustrated the proximity of neurovascular bundles within mineralized regions (**Figures 3A**,g). The localization of PGP 9.5 (b), OPN (c), OCN (d) (brown DAB stain counterstained with Gill's hematoxylin) (**Figure 3B**) in the extra cellular matrix of pulp was visualized using CLEM. Spatial association of PGP 9.5 immunolocalized nerves with α-SMA positive blood vessels are shown between light and SEM micrographs (**Figure 3C**). The immunolocalization of PGP 9.5 in the nerve bundles (PGP 9.5) and α-SMA in the blood vessels in association with OSX, BSP osteogenic molecules in the mineralized volumes (as asterisk showed in each image) within pulp (**Figure 3C**) were observed. However, OCN, OPN, BSP, and OSX, were not expressed in controls (unmineralized pulp) (**Supplementary Figure S1**).

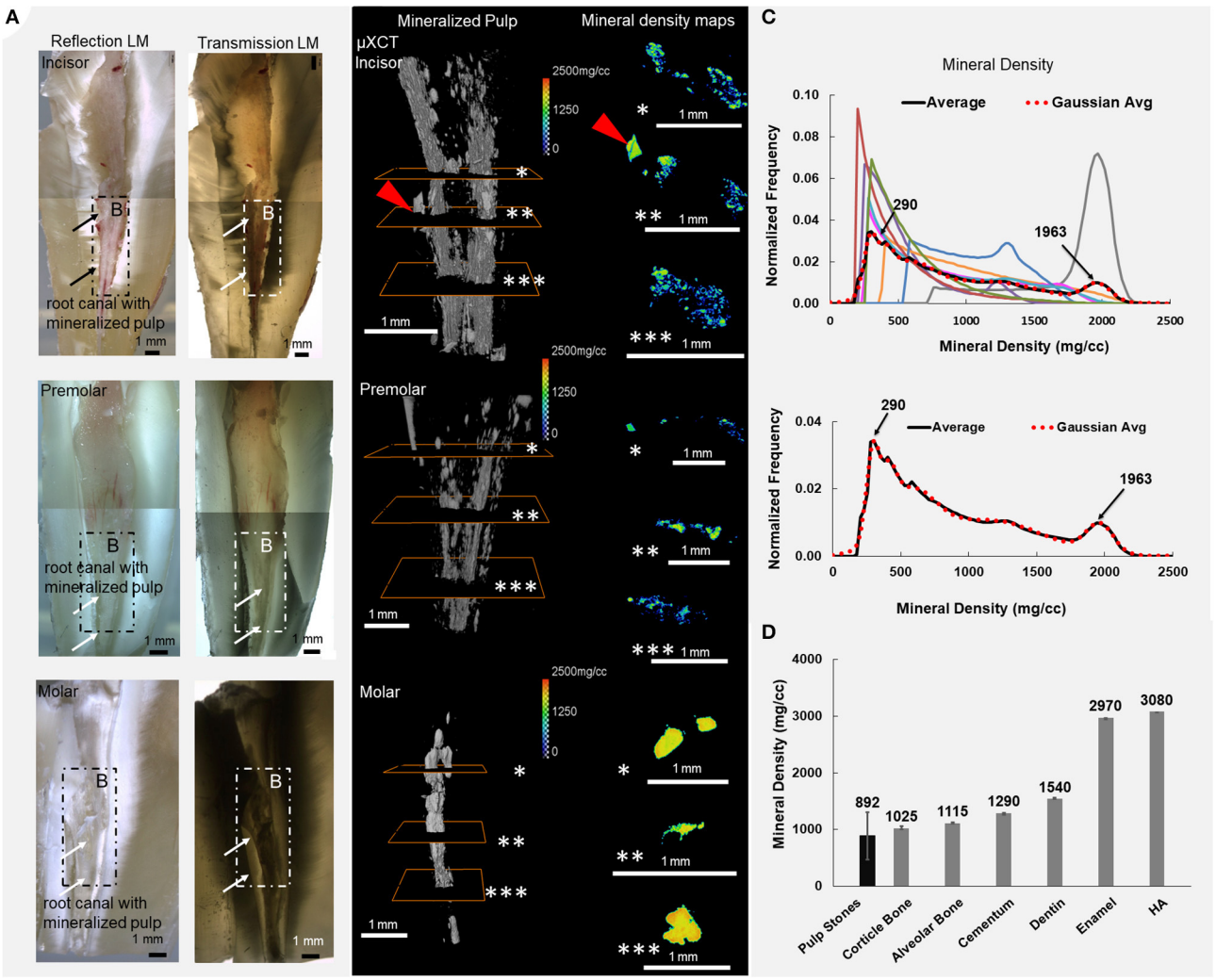

FIGURE 1 | The density of minerals in a unit volume of mineralizing pulp are heterogeneously distributed regardless of tooth type: the incisors, premolars, and molars. (A) Reflection and transmission light micrographs of sectioned teeth illustrate white and dark regions around the root canals (arrows point to the location of the pulp). **(B)** Varying mineral densities (MD) in digitally segmented volumes of mineralized pulp become apparent in the transverse sections (asterisks *, **, ***) of pulp (red arrowhead points to dentin-pulp interface—see **Figure 3**). **(C)** Normalized frequency of MD of pulp and **(D)** comparison of mineralized pulp and other mineralized tissues from humans including enamel, dentin, cementum, alveolar bone, hydroxyapatite (HA), and cortical bone are shown. The colored MD curves are patient-specific.

Surface Morphology and Structural Composition of Partially and Fully Mineralized Pulp

Diffused mineralization as noted previously by others also was observed in pulp (1). Nerves (N) and blood vessels (BV) were adjacent to mineralizing tissue that contained collagen fibrils with electron dense particles (red arrows, **Figure 4A**). Nanometer sized plate-like particles (**Figure 4A**), and aggregates of these plate-like particles in the macroscale mineralized collagenous constructs (red arrows, **Figure 4A**) were identified. The higher MD pulp contained mineralized bundles of organic tissue (**Figure 4B**), and collagen with intrafibrillar mineral (**Figure 4B**).

Correlative Microspectroscopy Using Micro XCT, and X-Ray Fluorescence Microprobe and Energy Dispersive X-Ray Spectroscopy Techniques

Mineralized regions of pulp expressed higher counts of Ca, P, and Zn (**Figure 5A**). Dentin expressed higher Ca and P, and higher counts of Zn at the DPI. Higher counts of Zn however, were observed in and within intact pulp in the DPC (**Figure 5B**). Atomic percentages of elements (Ca, P, Mg, Na, F, C, N, S, O) at locations 1, 2 and 3 are summarized in the table (**Figure 5A**). Ca and P counts inside pulp (location 1, pulp, green rectangle) were lower than those from intertubular (location 2), and mineralized particles within dentinal tubules (location 3).

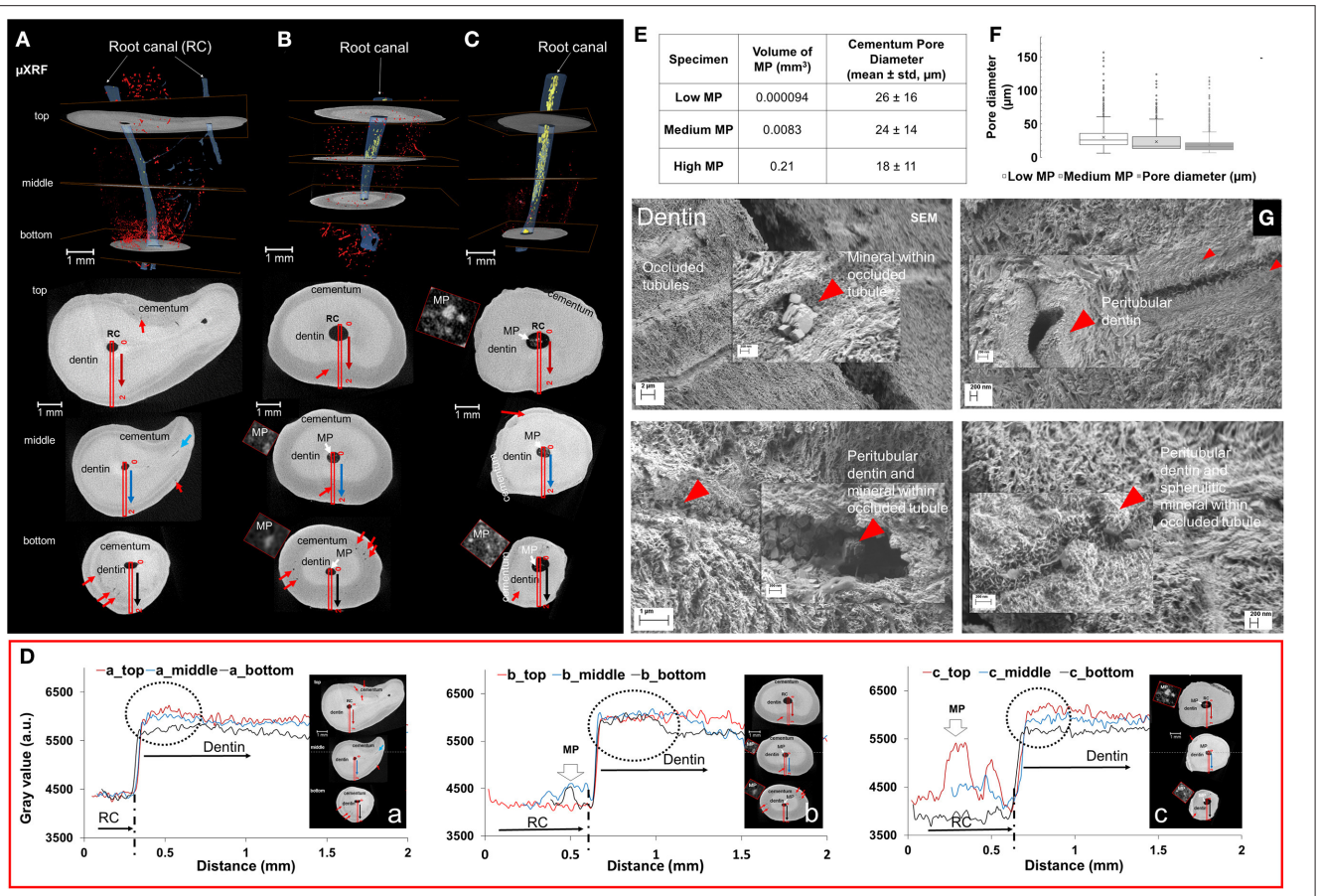

FIGURE 2 | Mineralizing tooth roots with decreased cementum and dentin porosities also contained pulp with higher mineral density. Root canals (blue), mineralizing pulp (white) **(A–C)**, and pores in cementum (red) with three X-ray slices (top, middle, bottom) from different roots **(A–C)** show the spatial relation between root canal system with mineralizing/mineralized pulp. Mineral density plot profiles from root canal to cementum expressed in gray scale illustrated higher mineral density regions (dotted circle, **D**) adjacent to the root canal, and various mineral density distributions and cementum thicknesses for different roots **(D)**. More lateral root canals and pores in cementum (red arrows in X-ray tomograms/top, middle and bottom sections) were observed in less mineralized pulp **(E,F)**. Tubules in dentin with nano/micro-mineralized occlusions (red arrowhead) were found adjacent to mineralizing pulp **(G)**.

However, elemental contents of intertubular dentin (location 2) and particles (location 3) within the dentinal tubules were similar. Atomic percentage of Mg in particles within the tubules (location 3) was higher than minerals in intertubular dentin (location 2) (**Figure 5A**).

Nano- and micro-spherical minerals in less mineralized regions and aggregates of mineralized spherical particles in regions with increasing mineral densities (**Figure 5B**) were observed. Phase analyses of maps 1–3 revealed the dominance of C in less mineralized regions (map 1), and Ca and P dominance in mineralizing regions (maps 2 and 3). More importantly, the particulates in map 1 contained Ca and P, and were phase separated from regions that were dominated with C counts. In maps 2 and 3, regions with higher counts of Ca and P, but lower C counts increased (**Figure 5B**). Atomic percentages of elements (Ca, P, Mg, Na, F, C, N, S, O, Zn) at these locations (map 1, map 2, and map 3) are summarized in **Figure 5**. Higher contents of Ca, P, Mg, and F also were detected in pulp with higher MD. Zn also was observed in pulp with relatively higher mineral density regions (**Figure 5**).

DISCUSSION

The sequelae that can help explain pathophysiology of tissues are often amiss. Pulp investigated in this study was from non-carious teeth that were extracted for orthodontic or prosthodontic reasons, with no *prior* information. The tissues of teeth are routinely subjected to insults in multiple ways. Acute and chronic tissue responses to insults (mechanical, chemical, and/or microbial loads) (1, 5, 12, 14) are often registered as spatial (macroscale DPC, microscale tissue/matrix/cell, and nanoscale particulate/biomoelcular levels) and temporal (short and long-term that can be connected to acute and chronic inflammatory cascades) adaptations. These adaptations are often mapped as changes in physicochemical, and biochemical

characteristics using multiple high resolution microscopy and spectroscopy techniques. Higher mineral densities but lower fracture resistance of dentin with age (27–30), decreased dentin permeability resulting from microbial attack (14, 31), and increased loss in tooth-sensitivity with increased cuspal attrition (5, 14) all are adapted characteristics of dentin. The white-reflecting and dark-opaque features in dentin encircling root canals in **Figure 1** indicated that, dentin indeed has adapted to conditions other than normal (1, 5, 12, 14, 31–35).

Although the spatial distribution of nerves in mammals has been documented to be tooth-function specific (36), consistent non-specificity of mineralized pulp to tooth type suggested that the biomineralization pathway need not be specific to tooth type (incisors to molars) and location (anterior to posterior) in the jaw. Despite, increased volumes of mineralized pulp were mostly observed in the apical portion (37) revealing a plausible macroscale effect of tooth architecture (37) on pulp mineralization.

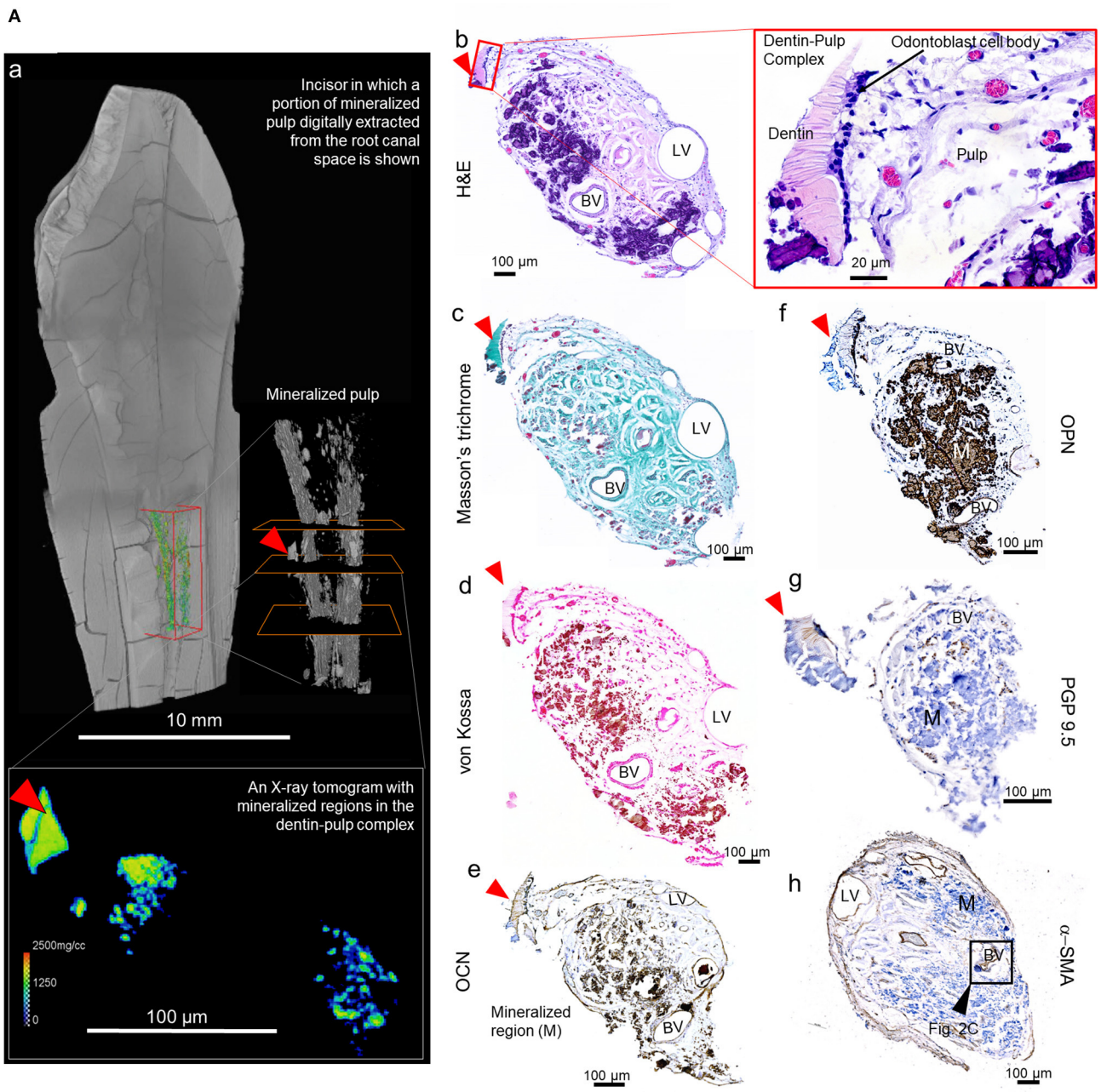

FIGURE 3 | Continued

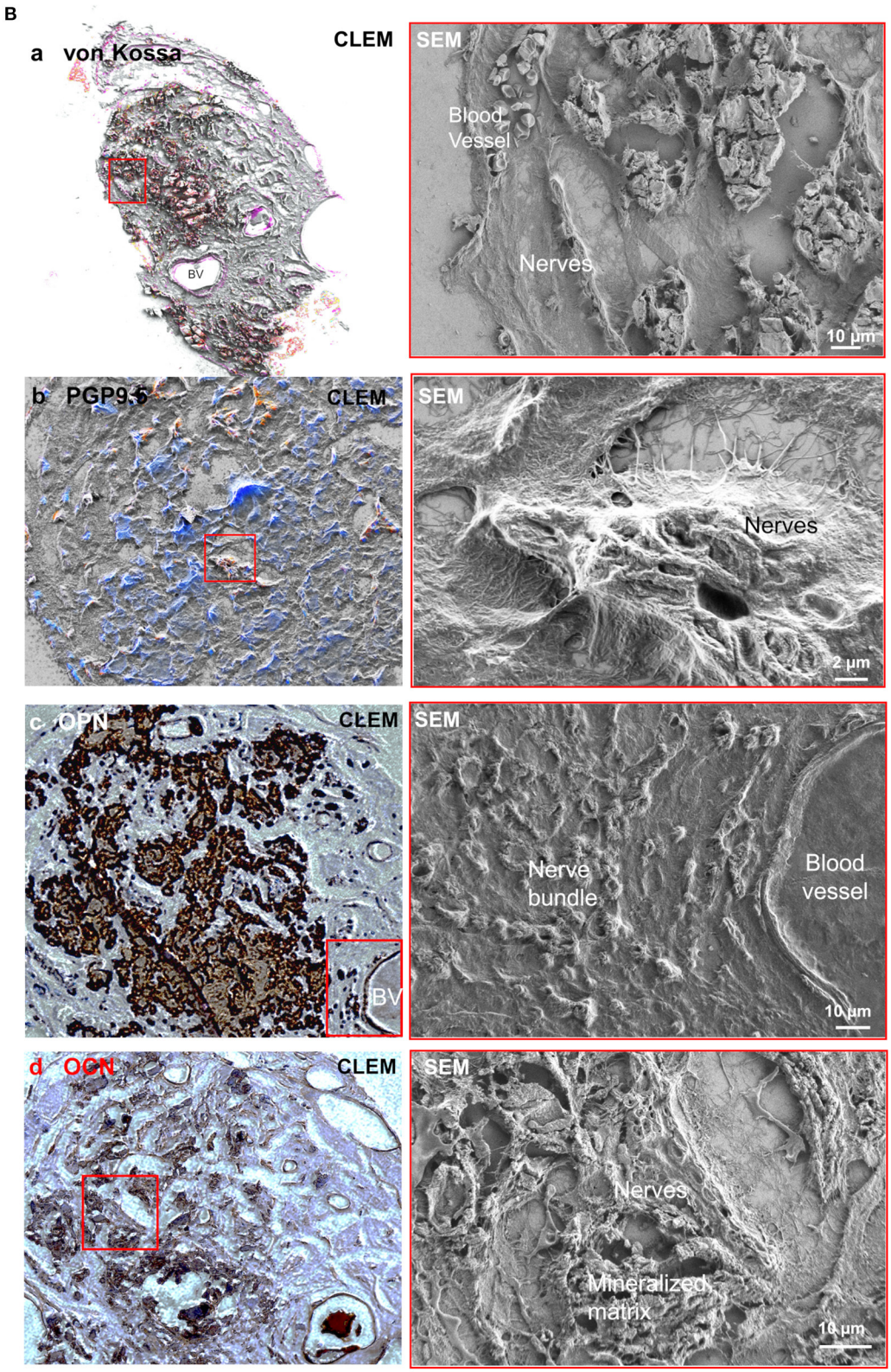

FIGURE 3 | Continued

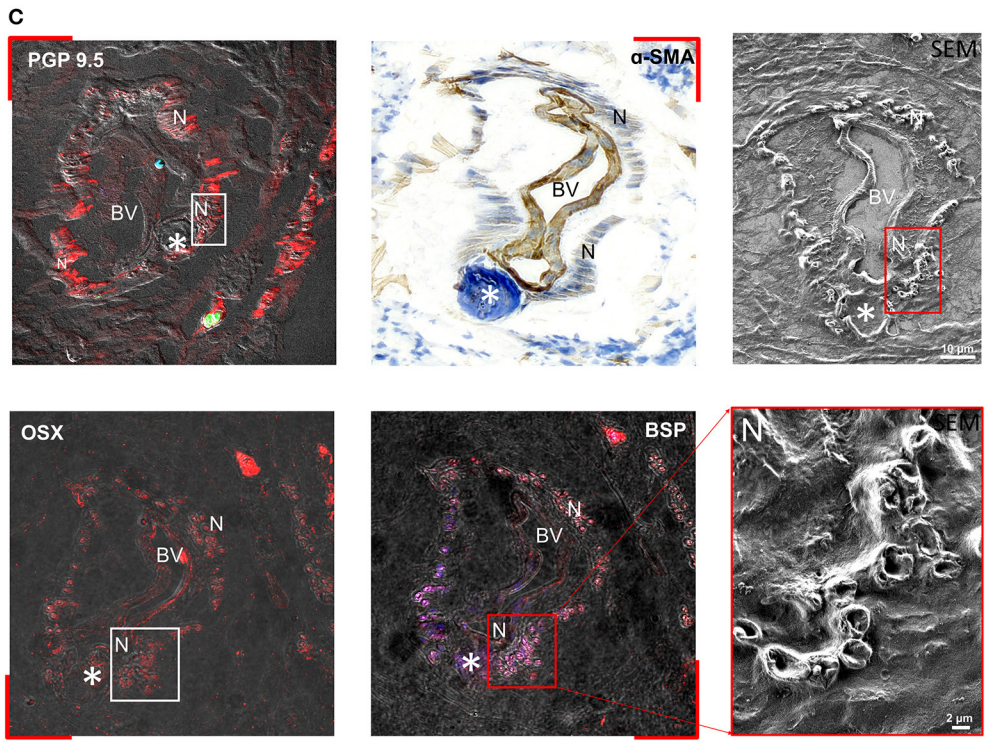

FIGURE 3 | Acidic molecules are contained within the minerals and the matrix of mineralizing pulp. (A) Digital volume illustrates the location of mineralized pulp (inside the box outlined in orange). (a) Minerals of varying densities are shown in transverse X-ray tomogram (outlined white rectangle) and corresponding histologic and immunohistologic sections with a visible dentin-pulp interface (red arrowhead) are shown (b–h). Light micrographs (LM) illustrate odontoblast cells relative to fibroblasts and other cells in the mineralizing matrix in hematoxylin and eosin (H&E, b; Red box contains dentin-pulp interface with corresponding cells), collagenous regions in Masson's trichrome (c), and mineralizing regions in von Kossa (d) stained sections. Osteocalcin (OCN, e), osteopontin (OPN, f), protein gene product 9.5 (PGP9.5, g), and α-smooth muscle actin (α-SMA, h) are localized in the blood vessels and nerves of the mineralizing pulp. **(B)** Histologic stains for mineral using von Kossa (a), and immunolocalization of PGP9.5 (b), OPN (c), and OCN (d) antigens are visible in the mineralized objects within the organic extracellular matrix of nerves and blood vessels. The corresponding extracellular matrix of the immunolocalized proteins are shown in electron micrographs to the right. **(C)** Nerve bundles (PGP 9.5) and blood vessels (α-SMA) in association with osteogenic molecules osterix and bone sialoprotein (OSX, BSP) within pulp were immunolocalized. BV, blood vessel; N, nerve; M, mineralizing tissue; LV, lymphatic vessels; red arrowhead points to the dentin-pulp interface (DPI). Immunolocalization of the same proteins, but in unmineralized pulp are shown in **Supplementary Figure S1**.

Much of pulp mineralization at a tooth-level or a DPC-level (macroscale) can be guided by fluid flow which is governed by the general laws of physics (Poiseuille's and Darcy's laws) (38, 39) and chemistry (van't Hoff's osmotic pressure and Fick's diffusion) (40, 41). These fundamental laws illustrate that for small changes in physical features such as root canal (R) radius, dentin tubule radius and length (r, L), interstitial fluid viscosity (μ), and concentrations of chemical constituents (C_1, C_2, C_n), significant shifts in pressure and chemical gradients can occur. These shifts in pressure and chemical gradients can alter the rates of volume flow across a unit area of a tissue. Based on the structural interconnectedness between dentin and pulp, and dentin and cementum (15), the observed changes in dentin (particulate growth and/or increased pertubular dentin production) and cementum (decreased permeabilities) could result in changes in interstitial fluid pressure (4, 42, 43) of the softer pulp. These laws also explain that changes in (1) pressure and chemical gradients at a tooth-level and (2) dentin and cementum permeabilities at a tissue-level can "drive" the rates of heterogenous and/or homogenous nucleation and subsequent mineralization of an organic matrix even in the absence of cells (44, 45) (**Figure 6**). Fundamental physical chemistry experiments have illustrated that osteogenic molecules such as OCN and BSP in the absence of cells can act as nucleators and in association with collagen can facilitate heterogeneous nucleation, and apatite formation (44, 45). Collectively, these changes in physicochemical, and biochemical chactersitics revealed the interconnected vulnerabilities between the seemingly disparate hard and soft tissues even in the absence of cells.

In the presence of cells, the observed correlations between physical and chemical features (**Figure 2**) of dentin, cementum, and pulp revealed macroscale culprits that could potentiate microanatomical self-governing regions (**Figures 1**, **2**) in the insulted pulp. The narrowed orifice at the root-tip also can potentiate the already inflammed pulp via capillary stragulation (4). However, in a partially mineralized pulp at locations farther away from the sphere of influence of insults (top, middle, bottom sections, **Figure 4**), the built-in control system

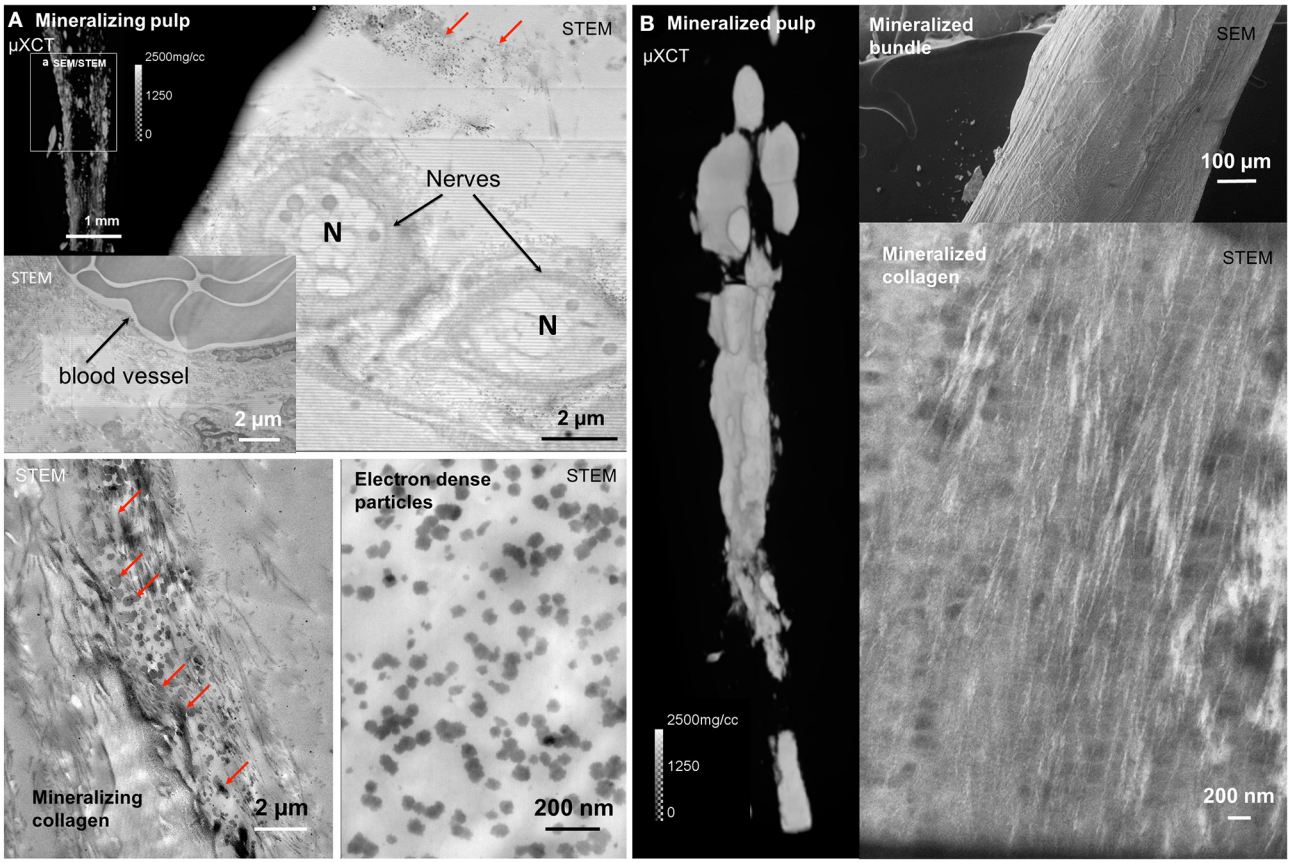

FIGURE 4 | Blood vessels, nerves, electron dense particulates, and collagen with intrafibrillar mineral are contained in partially and fully mineralized pulp. (A) Cells, blood vessels, and nerves were observed within mineralizing pulp (red arrows). **(B)** Dense collagen bundles with collagen fibrils and electron dense particles also were observed in macroscale mineralizing and mineralized collagenous pulp.

can "erase" the initial inflammatory effects of the insults and reverse the local interstitial fluid pressures to homeostasis. On the other hand, chronic response to sustained insults can "tip" this balance toward a sustained inflammatory mode, and consequently an irreversible state. The subsequent changes in pressure gradients at the tissue and organ levels can contribute to various mechano- and chemo-biological events, and plausibly, different biomineralization pathways. Specifically, the most noted mechano-chemo-sensing biomineralization pathways involve the production of osteogenic proteins as nucleators (46–49) through (1) increased vasodilation by "mechanically strained" endothelial cells (4, 50, 51); (2) compromised capillary pressures and pericyte stimulation (50, 52) resulting in a sustained increase in interstitial fluid pressure within the pulp; and (3) capillary strangulation resulting in hypoxic conditions and reactive oxygen species (ROS) (4, 53).

Studies have already shown an obvious reduction of pulpal blood flow and marked histologic changes in the pulp as a result of intrusive orthodontic forces (16); pulp canal obliteration appears to be a sequel to revascularization and/or reinnervation of a damaged pulp after traumatic injury (54). Inflammatory biomarkers including matrix metalloproteases and neuropeptides are released by traumatic, orthodontic, thermal, and chemical insults. The function of MMPs and neuropeptides are dependent on the catalytic or co-factor functions of various heavy metals including Zn^{2+} (55–59). Increased expressions of neuropeptides including calcitonin gene-related peptide (CGRP) can alter vascular function and interstitial fluid pressure, but do so locally within the tissues of the pulp (60). The finding of silver nitrate (von Kossa) positive minerals around the α-SMA positive blood vessels and PGP 9.5 positive nerves (**Figure 2B**) is suggestive of neurovascular involvement, a potential culprit in pathophysiology of pulp tissue mineralization.

Localization of SIBLING proteins, OPN and BSP, and OCN around α-SMA vasculature and PGP 9.5 positive nerves, furthermore provided insights into the plausible roles of neurovasculature and osteogenic proteins (61, 62) on controlled mineralization of collagen albeit pathologic in nature. SIBLINGs express themselves in regions that are mechanically challenged, not necessarily as mineral forming, but also as mineral inhibiting proteins. OPN is one such plasma protein whose intrinsic function as an inhibitor of mineralization also is central to

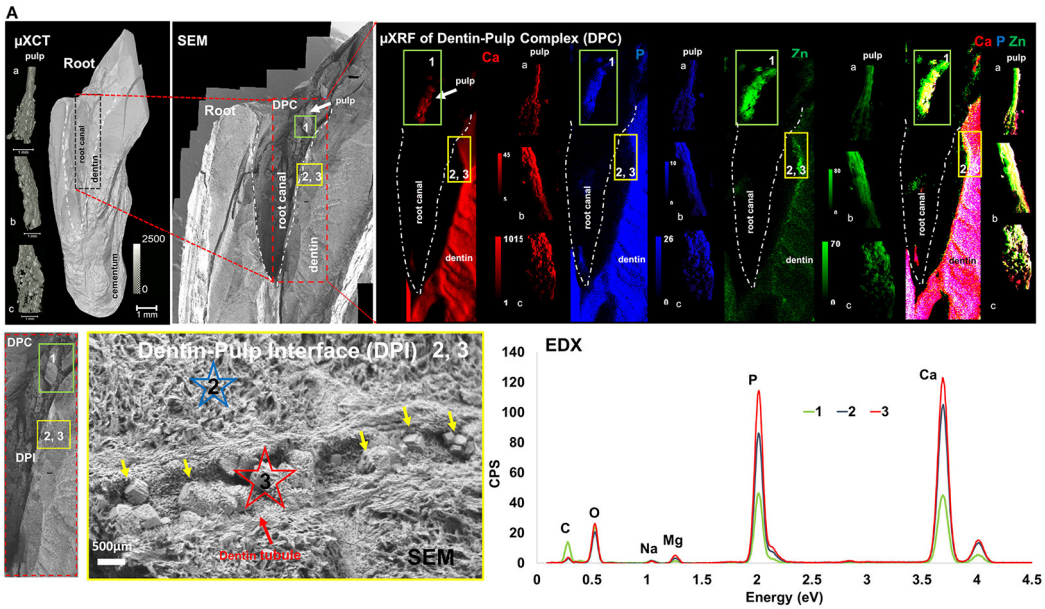

Atom%	Ca	P	Mg	Na	F	C	N	S	O
1	17.43	9.17	0.42	0.66	0.90	23.43	5.79	0.09	42.09
2	36.7	15.72	0.80	0.50	0.26	4.40	1.40	0.08	40.15
3	35.08	16.89	0.99	0.29	0	4.61	1.66	0.08	40.40

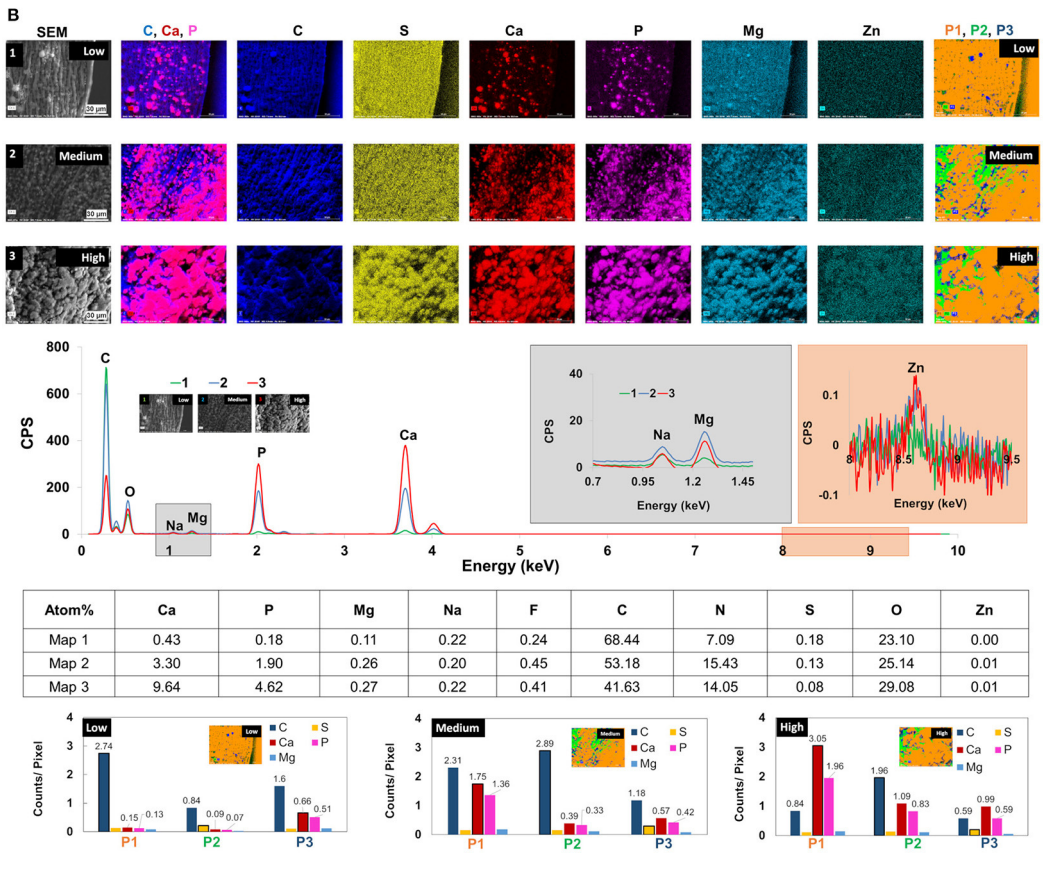

Atom%	Ca	P	Mg	Na	F	C	N	S	O	Zn
Map 1	0.43	0.18	0.11	0.22	0.24	68.44	7.09	0.18	23.10	0.00
Map 2	3.30	1.90	0.26	0.20	0.45	53.18	15.43	0.13	25.14	0.01
Map 3	9.64	4.62	0.27	0.22	0.41	41.63	14.05	0.08	29.08	0.01

FIGURE 5 | Zinc and magnesium were co-localized in dentin-pulp complex (DPC). In particular, trace elements were colocalized at the dentin-pulp interface (DPI), within mineralized pulp, and in tubular occlusions within dentin. (A) (Top row, Left to right) Spatial maps of heterogeneous mineral densities (micro-XCT), matrix structure Dentin-pulp interface - DPI and regions 1-3, SEM), and element counts (calcium, phosphorus, magnesium and zinc counts) of root canal

(Continued)

FIGURE 5 | (outlined in dashed lines) and pulp from three different patients (left, volumes of pulp—a–c) are shown. DPI (yellow box, XRF maps) express higher zinc and calcium counts, but pulp (green box) also contains phosphorus (regions of white in green box, and pulp a–c, right). (Middle row, Left to right) The DPI with dentin and its occluded tubule contains particulates (yellow arrows) with higher Mg counts (red star at location 3, red graph to the right). Inter-tubular dentin however, contains lower Mg (blue star at location 2, blue graph to the right) counts but higher than Zn-rich mineralized pulp. (Bottom row) Atomic percentages of elements at locations (1, 2, and 3) are shown in the table. Ca and P contents of location 1 are different from those at locations 2 and 3, and elemental contents of 2 and 3 are similar. Atomic percentage of Mg at location 3 is slightly higher than location 2. **(B)** Top three rows: Spatial elemental maps from regions 1 (low), 2 (medium) and 3 (high) mineralized extracted pulp contain spherulitic minerals of higher counts of C in less mineralized regions, and aggregates of these spherulitic minerals with higher counts of Zn, Ca, P, and Mg in more mineralized regions of the same pulp. Fourth row: X-ray spectra illustrate energy peaks of elements (Ca, P, Mg, Na, F, C, N, S, O, Zn) from lower (1), medium (2) and higher (3) mineral density regions. Atomic percentages of elements at these locations in maps 1–3 are summarized in table (fifth row). Bottom row (bar charts): Principal component analysis illustrated phases 1, 2 and 3 (P1–P3) in lower, medium and higher mineral density regions of pulp with significant variances in C, P, Ca, S, and Mg. The first phase P1 accounts for more than 70% of the variance in lower, medium, and higher mineral density regions of pulp. In the lower mineral density pulp in map 1, C counts per pixel are the highest in P1 (yellow). With increasing mineral density of pulp, Ca and P counts per pixel are highest in P3 (blue) for map1, and highest in P1 for maps 2 and 3; S counts per pixel are highest in P2 (green) for map1, and P3 for maps 2 and 3. XRF units are in counts; mineral density units are in mg/cc; CPS, counts *per second*.

the biomineralization pathway; its involvement could be to control mineral growth albeit pathologic as discussed in various studies *in vitro* and *in vivo* (44, 45, 63, 64). Electron dense particles (**Figure 3**) and diffused nanometer sized plate-like minerals located within the macroscale mineralizing collagenous constructs, and as intrafibrillar mineral (**Figure 3A**) confirmed heterogeneous nucleation within pulp. OCN is expressed in fibroblast-like cells of the pulp (65), and has been shown to influence specifically intrafibrillar mineralization of collagen (66). OSX is a Zn finger transcription factor and plays an important role in pre-differentiated osteoblasts (67). As an upstream marker in the osteogenic signaling pathway, OSX also could modulate the expressions of OPN, OCN, and the more downstream marker BSP (67, 68). However, we contend that its presence is more central to the nerve, as data alludes to pulp mineralization as ectopic mineralization, and not necessarily heterotopic ossification (no osteocytes were observed).

It should not come too much as a surprise that Zn was observed, as its localization is central to most sterile and non-sterile inflammatory pathways. Inflammation encourages vesicular transport of Zn and Mg or as bions in biological fluids (48, 69, 70). These spherulitic structures also could be associated with local tissue mineralization (**Figure 5**). Additionally, extracellular spherulitic bodies including exosomal and apoptotic bodies with sizes ranging from $<$50 nm to greater than microns continue to be observed in vascular plaques in multiple anatomical locations in humans (heart, kidney, brain) (71–75). However, studies identifying mechanisms of interaction between extracellular vesicles and collagen driving the formation of micro/macro mineralization in tissue constructs are warranted.

Zn also is involved in downstream biomineralization events especially related to hypoxia induced by ischemia (i.e., HIF, NF-κB) (53, 76–79); all of which condition the tissue biochemistry and facilitate passive or active recruitment of Ca^{2+} and PO_4^{3-} ions. Changes in interstitial fluid pressure can alter hemodynamic and vascular mechanotransduction, induce osteogenic protein production, shift oxygen tension, and generate ROS. Further research on hemodynamic force-induced inflammation in association with ROS facilitated by Zn will be necessary to elucidate yet another mechanism of pathologic mineralization, but under ischemic conditions [oxygen tension resulting from insufficient blow flow, specifically capillary strangulation (2, 4) at the root apices]. Given all the many discussed pathways that would result in pathologic biominerals in pulp, confirmation of highly probable pathways at local tissue- and tooth-levels through niche-specific simulation studies are highly warranted.

CONCLUSION

Spatial colocalization of physicochemical and biomolecular compositions of biominerals in an already existing neurovascular pulpal matrix, suggest primary and secondary biomineralization pathways. Primary pathways are specific to the tissues of the pulp and dentin, and secondary pathways are defined by the aggregate effects of the primary but at an organ level. Primary pathways include shifts in hemodynamic and interstitial fluid pressures also by sterile stimuli (i.e., mechanical, chemical, thermal) that illicit neurogenic inflammation, a process that could alter normal neural and vascular functions. These shifts in tissue compliance resulting from interstitial fluid pressure change also can differentiate various cells including pericytes, endothelial, and other resident stem cells into an osteogenic lineage and consequently promote biomineralization locally within the pulp. Reduction in permeability and oxygen tension resulting from occluded dentin tubules and lateral canals, and altered tooth architecture can further stimulate ischemic events and ROS. The presence of Zn expressions in mineralized pulp is further suggestive of Zn-related biochemical pathways being central to mineralization of the DPC. Regardless, mapping niche-specific upstream and downstream biomarkers are critical toward formulating functional assays that would guide translational approaches to mitigate primary and secondary pathologic biomineralization pathways. Furthermore, from a clinical viewpoint, these observations in pulp underpin the short and long-term prognosis of a tooth receiving anesthetic, restorative, periodontal, and/or orthodontic treatment, and can inform clinicians

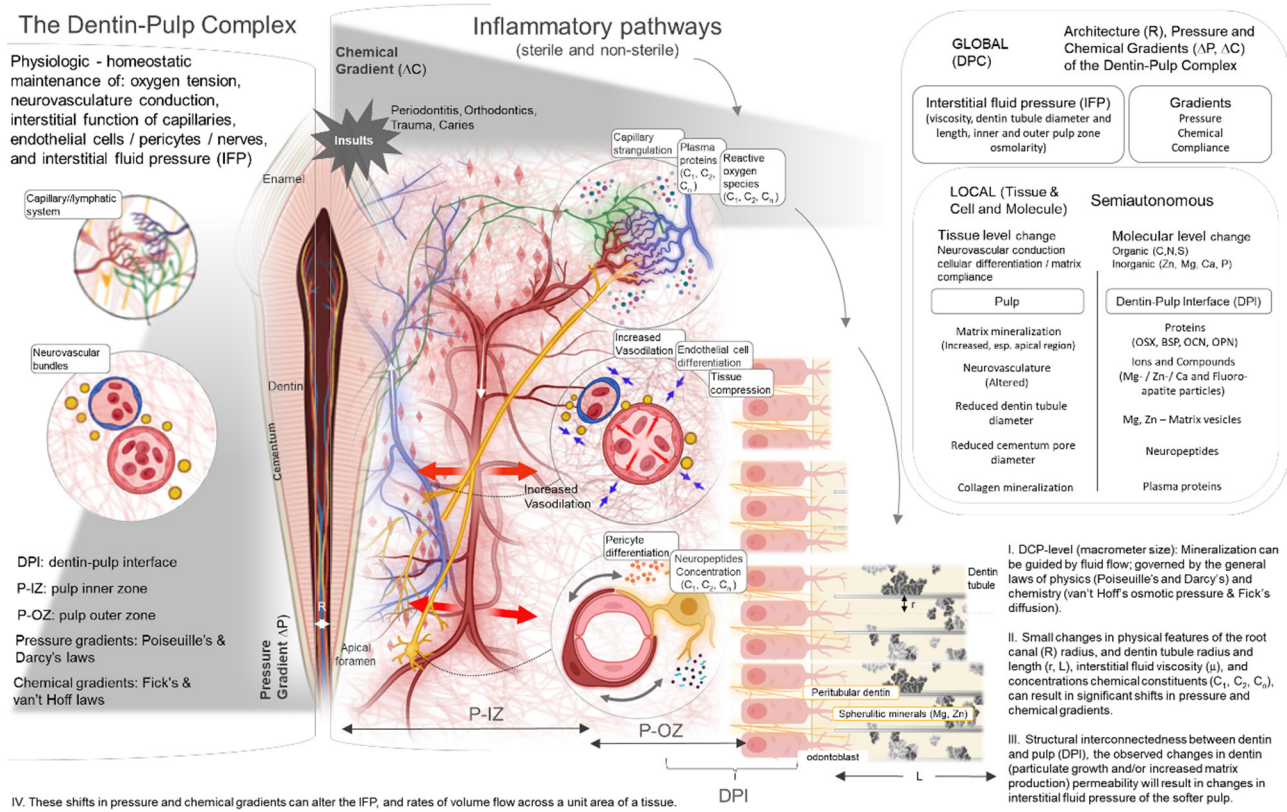

FIGURE 6 | Insights into Pulp Biomineralization Pathways: **(I)** DPC-level (macrometer size): Mineralization can be guided by fluid flow; governed by the general laws of physics (Poiseuille's and Darcy's) and chemistry (van't Hoff's osmotic pressure & Fick's diffusion). **(II)** Small changes in physical features of the root canal (R) radius, and dentin tubule radius and length (r, L), interstitial fluid viscosity (μ), and concentrations chemical constituents (C_1, C_2, C_n), can result in significant shifts in pressure and chemical gradients. **(III)** Structural interconnectedness between dentin and pulp (DPI), the observed changes in dentin (particulate growth and/or increased matrix production) permeability will result in changes in interstitial fluid pressure of the softer pulp. **(IV)** These shifts in pressure and chemical gradients can alter the IFP, and rates of volume flow across a unit area of a tissue. **(V)** These laws also explain that changes in 1) pressure and chemical gradients at a tooth-level, and 2) dentin permeabilities at a tissue-level can "drive" the rates of heterogenous and/or homogenous nucleation and subsequent mineralization of an organic matrix even in the absence of cells.

the subtleties related to pulpitis, dentin-bridge, and pulp stone formation.

DATA AVAILABILITY STATEMENT

The original contributions presented in the study are included in the article/**Supplementary Material**, further inquiries can be directed to the corresponding author.

ETHICS STATEMENT

The studies involving human participants were reviewed and approved by Human Research Protection Program Institutional Review Board of UCSF (Study Number: 16-19606). Written informed consent for participation was not required for this study in accordance with the national legislation and the institutional requirements.

AUTHOR CONTRIBUTIONS

RH contributed to study design, data acquisition, in particular, immunohistochemistry, electron microscopy, and correlative light and electron microscopy. CC contributed to clinical input, editing, and preparing **Figure 6**. MS contributed to editing. MK contributed to writing, data acquisition, analysis, interpretation of data specific to micro CT related scans, energy dispersive X-ray analysis, and correlative microscopy. SH contributed to study design, data interpretation, prepared **Figure 6**, wrote, edited, revised, and critically reviewed the manuscript with all authors. All authors gave final approval and agree to be accountable for all aspects of the work.

FUNDING

This research was funded by the Program in Biomineralization Studies (PiBiomS), Departments of Preventive and Restorative Dental Sciences, and Urology, Schools of Dentistry and Medicine, UCSF. PiBiomS is a partnership between the Schools of Dentistry and Medicine at UCSF to investigate the cause of various pathologic biominerals in humans.

ACKNOWLEDGMENTS

The authors thank Dr. Sulyanto for her feedback and clinical input. The authors thank Ms. Grace Nonomura for her help in specimen preparation, and the Biomaterials and Bioengineering Correlative Microscopy Core (http://bbcmc.ucsf.edu), UCSF for the use of their MicroXCT-200 and SIGMA 500-VP Field Emission Electron Microscope—Scanning and Transmission. This research used beamline 10.3.2 of the Advanced Light Source, a Department of Energy Office of Science user facility under contract DE-AC02-05CH11231. The authors would like to acknowledge Dr. Sirine Fakra for her help and assistance at beamline 10.3.2. **Figure 6** was partly generated using icons in Biorender.com.

SUPPLEMENTARY MATERIAL

The Supplementary Material for this article can be found online at: https://www.frontiersin.org/articles/10.3389/fdmed.2022.883336/full#supplementary-material

Supplementary Figure S1 | Immunostains for OCN, OPN, BSP, and OSX in unmineralized pulp.

Supplementary Movie S1 | Movie illustrates pulp from three patients. Left to right illustrate low (control), medium, and high mineral densities of pulp, along with dentin and cementum respectively.

REFERENCES

1. Keijo L, Paivi K, Inge F, Ellen B. Structure and Function of the Dentin-Pulp Complex. In: *Cohen's Pathways of the Pulp*. 11th ed. St. Louis, MI: Elsevier (2020).
2. Heyeraas KJ. Pulpal hemodynamics and interstitial fluid pressure: balance of transmicrovascular fluid transport. *J Endod.* (1989) 15:468–72. doi: 10.1016/S0099-2399(89)80026-3
3. Berggreen E, Wiig H, Virtej A. Fluid transport from the dental pulp revisited. *Eur J Oral Sci.* (2020) 128:365–8. doi: 10.1111/eos.12733
4. Heyeraas KJ, Berggreen E. Interstitial fluid pressure in normal and inflamed pulp. *Crit Rev Oral Biol Med.* (1999) 10:328–36. doi: 10.1177/10454411990100030501
5. Pashley DH. Dynamics of the pulpo-dentin complex. *Crit Rev Oral Biol Med.* (1996) 7:104–33. doi: 10.1177/10454411960070020101
6. Brannstrom M, Linden LA, Astrom A. The hydrodynamics of the dental tubule and of pulp fluid. A discussion of its significance in relation to dentinal sensitivity. *Caries Res.* (1967) 1:310–7. doi: 10.1159/000259530
7. Brannstrom M. The hydrodynamics of the dental tubule and pulp fluid: its significance in relation to dentinal sensitivity. *Annu Meet Am Inst Oral Biol.* (1966) 23:219.
8. Goga R, Chandler NP, Oginni AO. Pulp stones: a review. *Int Endod J.* (2008) 41:457–68. doi: 10.1111/j.1365-2591.2008.01374.x
9. Bastos JV, Cortes MIS. Pulp canal obliteration after traumatic injuries in permanent teeth - scientific fact or fiction? *Braz Oral Res.* (2018) 32:e75. doi: 10.1590/1807-3107bor-2018.vol32.0075
10. Min KS, Park HJ, Lee SK, Park SH, Hong CU, Kim HW, et al. Effect of mineral trioxide aggregate on dentin bridge formation and expression of dentin sialoprotein and heme oxygenase-1 in human dental pulp. *J Endod.* (2008) 34:666–70. doi: 10.1016/j.joen.2008.03.009
11. Cate T, Nanci A. *Ten Cate's - Oral Histology: Development, Structure, and Function*. St. Louis, MI: Elsevier (2013).
12. Wisniewska K, Rybak Z, Szymonowicz M, Kuropka P, Dobrzynski M. Review on the lymphatic vessels in the dental pulp. *Biology.* (2021) 10:1257. doi: 10.3390/biology10121257
13. Durham AL, Speer MY, Scatena M, Giachelli CM, Shanahan CM. Role of smooth muscle cells in vascular calcification: implications in atherosclerosis and arterial stiffness. *Cardiovasc Res.* (2018) 114:590–600. doi: 10.1093/cvr/cvy010
14. Pashley DH. Dentin-predentin complex and its permeability: physiologic overview. *J Dent Res.* (1985) 64 Spec No:613–20. doi: 10.1177/002203458506400419
15. Petelin M, Skaleric U, Cevc P, Schara M. The permeability of human cementum in vitro measured by electron paramagnetic resonance. *Arch Oral Biol.* (1999) 44:259–67. doi: 10.1016/S0003-9969(98)00124-1

16. Bauss O, Rohling J, Rahman A, Kiliaridis S. The effect of pulp obliteration on pulpal vitality of orthodontically intruded traumatized teeth. *J Endod.* (2008) 34:417–20. doi: 10.1016/j.joen.2008.01.006
17. Ustriyana P, Hennefarth MR, Srirangapatanam S, Jung H, Wang Y, Chen L, et al. Mineralized Peyronie's plaque has a phenotypic resemblance to bone. *Acta Biomater.* (2022) 140:457–66. doi: 10.1016/j.actbio.2021.11.025
18. Wang Y, Chen L, Kang M, Ling L, Tian F, Won-Kim SH, et al. The fracture callus is formed by progenitors of different skeletal origins in a site-specific manner. *JBMR plus.* (2019) 3:e10193. doi: 10.1002/jbm4.10193
19. Sherer BA, Chen L, Kang M, Shimotake AR, Wiener SV, Chi T, et al. A continuum of mineralization from human renal pyramid to stones on stems. *Acta Biomater.* (2018) 71:72–85. doi: 10.1016/j.actbio.2018.01.040
20. Lin JD, Ryder M, Kang M, Ho SP. Biomechanical pathways of dentoalveolar fibrous joints in health and disease. *Periodontol 2000.* (2020) 82:238–56. doi: 10.1111/prd.12306
21. Ho SP, Chen L, Allen FI, Hsi RS, Shimotake AR, Wiener SV, et al. Architecture-Guided fluid flow directs renal biomineralization. *Sci Rep.* (2018) 8:14157. doi: 10.1038/s41598-018-30717-x
22. Li L, Zhu YQ, Jiang L, Peng W, Ritchie HH. Hypoxia promotes mineralization of human dental pulp cells. *J Endod.* (2011) 37:799–802. doi: 10.1016/j.joen.2011.02.028
23. Sundell JR, Stanley HR, White CL. The relationship of coronal pulp stone formation to experimental operative procedures. *Oral Surg Oral Med Oral Pathol.* (1968) 25:579–89. doi: 10.1016/0030-4220(68)90303-4
24. Gautam S, Galgali SR, Sheethal HS, Priya NS. Pulpal changes associated with advanced periodontal disease: a histopathological study. *J Oral Maxillofac Pathol.* (2017) 21:58–63. doi: 10.4103/0973-029X.203795
25. Djomehri SI, Candell S, Case T, Browning A, Marshall GW, Yun W, et al. Mineral density volume gradients in normal and diseased human tissues. *PLoS ONE.* (2015) 10:e0121611. doi: 10.1371/journal.pone.0121611
26. Yang L, Kang M, He R, Meng B, Pal A, Chen L, et al. Microanatomical changes and biomolecular expression at the PDL-entheses during experimental tooth movement. *J Periodontal Res.* (2019) 54:251–8. doi: 10.1111/jre.12625
27. Yan W, Montoya C, Oilo M, Ossa A, Paranjpe A, Zhang H, et al. Reduction in fracture resistance of the root with aging. *J Endod.* (2017) 43:1494–8. doi: 10.1016/j.joen.2017.04.020
28. Montoya C, Arola D, Ossa EA. Importance of tubule density to the fracture toughness of dentin. *Arch Oral Biol.* (2016) 67:9–14. doi: 10.1016/j.archoralbio.2016.03.003
29. Montoya C, Arango-Santander S, Pelaez-Vargas A, Arola D, Ossa EA. Effect of aging on the microstructure, hardness and chemical composition of dentin. *Arch Oral Biol.* (2015) 60:1811–20. doi: 10.1016/j.archoralbio.2015.10.002
30. Ivancik J, Majd H, Bajaj D, Romberg E, Arola D. Contributions of aging to the fatigue crack growth resistance of human dentin. *Acta Biomater.* (2012) 8:2737–46. doi: 10.1016/j.actbio.2012.03.046
31. Fusayama T, Okuse K, Hosoda H. Relationship between hardness, discoloration, and microbial invasion in carious dentin. *J Dent Res.* (1966) 45:1033–46. doi: 10.1177/00220345660450040401
32. Sourai PG. [Microbial permeability of dentin]. *Stomatologia.* (1989) 46:359–72.
33. Pashley DH, Pashley EL, Carvalho RM, Tay FR. The effects of dentin permeability on restorative dentistry. *Dent Clin North Am.* (2002) 46:211–45, v–vi. doi: 10.1016/S0011-8532(01)00009-X
34. Nissan R, Segal H, Pashley D, Stevens R, Trowbridge H. Ability of bacterial endotoxin to diffuse through human dentin. *J Endod.* (1995) 21:62–4. doi: 10.1016/S0099-2399(06)81096-4
35. Fusayama T, Terashima S. Differentiation of two layers of carious dentin by staining. *Bull Tokyo Med Dent Univ.* (1972) 19:83–92.
36. Trulsson M, Johansson RS. Orofacial mechanoreceptors in humans: encoding characteristics and responses during natural orofacial behaviors. *Behav Brain Res.* (2002) 135:27–33. doi: 10.1016/S0166-4328(02)00151-1
37. Brown AC, Yankowitz D. Tooth pulp tissue pressure and hydraulic permeability. *Circ Res.* (1964) 15:42–50. doi: 10.1161/01.RES.15.1.42
38. Pfitzner J. Poiseuille and his law. *Anaesthesia.* (1976) 31:273–5. doi: 10.1111/j.1365-2044.1976.tb11804.x
39. Niven RK. A derivation of Darcy's law. *Ground Water.* (2002) 40:670–1; discussion 1–2. doi: 10.1111/j.1745-6584.2002.tb02554.x
40. Miki K, Sagawa S, Shiraki K. Factors influencing the determination of colloid osmotic pressure of plasma. *J UOEH.* (1983) 5:405–12. doi: 10.7888/juoeh.5.405
41. Su J, Zhao Y, Fang C, Shi Y. Asymmetric osmotic water permeation through a vesicle membrane. *J Chem Phys.* (2017) 146:204902. doi: 10.1063/1.4983749
42. Matthews B, Andrew D. Microvascular architecture and exchange in teeth. *Microcirculation.* (1995) 2:305–13. doi: 10.3109/10739689509148275
43. Heyeraas KJ. Micropuncture measurements of interstitial fluid and vascular pressures in dental pulp. *Int Endod J.* (1993) 26:15–6. doi: 10.1111/j.1365-2591.1993.tb00537.x
44. Veis A, Dorvee JR. Biomineralization mechanisms: a new paradigm for crystal nucleation in organic matrices. *Calcif Tissue Int.* (2013) 93:307–15. doi: 10.1007/s00223-012-9678-2
45. George A, Veis A. Phosphorylated proteins and control over apatite nucleation, crystal growth, and inhibition. *Chem Rev.* (2008) 108:4670–93. doi: 10.1021/cr0782729
46. Cui L, Houston DA, Farquharson C, MacRae VE. Characterisation of matrix vesicles in skeletal and soft tissue mineralisation. *Bone.* (2016) 87:147–58. doi: 10.1016/j.bone.2016.04.007
47. Kirsch T. Determinants of pathological mineralization. *Curr Opin Rheumatol.* (2006) 18:174–80. doi: 10.1097/01.bor.0000209431.59226.46
48. Golub EE. Biomineralization and matrix vesicles in biology and pathology. *Semin Immunopathol.* (2011) 33:409–17. doi: 10.1007/s00281-010-0230-z
49. Weidemann A, Breyer J, Rehm M, Eckardt KU, Daniel C, Cicha I, et al. HIF-1alpha activation results in actin cytoskeleton reorganization and modulation of Rac-1 signaling in endothelial cells. *Cell Commun Signal.* (2013) 11:80. doi: 10.1186/1478-811X-11-80
50. Shroff RC, Shanahan CM. The vascular biology of calcification. *Semin Dial.* (2007) 20:103–9. doi: 10.1111/j.1525-139X.2007.00255.x
51. Tyson J, Bundy K, Roach C, Douglas H, Ventura V, Segars MF, et al. Mechanisms of the osteogenic switch of smooth muscle cells in vascular calcification: WNT signaling, BMPs, mechanotransduction, and EndMT. *Bioengineering.* (2020) 7:88. doi: 10.3390/bioengineering7030088
52. Kapustin AN, Chatrou ML, Drozdov I, Zheng Y, Davidson SM, Soong D, et al. Vascular smooth muscle cell calcification is mediated by regulated exosome secretion. *Circ Res.* (2015) 116:1312–23. doi: 10.1161/CIRCRESAHA.116.305012
53. Slepchenko KG, Lu Q, Li YV. Cross talk between increased intracellular zinc (Zn(2+)) and accumulation of reactive oxygen species in chemical ischemia. *Am J Physiol Cell Physiol.* (2017) 313:C448–59. doi: 10.1152/ajpcell.00048.2017
54. Andreasen FM, Zhijie Y, Thomsen BL, Andersen PK. Occurrence of pulp canal obliteration after luxation injuries in the permanent dentition. *Endod Dent Traumatol.* (1987) 3:103–15. doi: 10.1111/j.1600-9657.1987.tb00611.x
55. Maret W. Zinc in cellular regulation: the nature and significance of "zinc signals". *Int J Mol Sci.* (2017) 18:2285. doi: 10.3390/ijms18112285
56. Finney LA, O'Halloran TV. Transition metal speciation in the cell: insights from the chemistry of metal ion receptors. *Science.* (2003) 300:931–6. doi: 10.1126/science.1085049
57. Rink L, Gabriel P. Zinc and the immune system. *Proc Nutr Soc.* (2000) 59:541–52. doi: 10.1017/S0029665100000781
58. McCall KA, Huang C, Fierke CA. Function and mechanism of zinc metalloenzymes. *J Nutr.* (2000) 130:1437S−46. doi: 10.1093/jn/130.5.1437S
59. Wuthier RE, Lipscomb GF. Matrix vesicles: structure, composition, formation and function in calcification. *Front Biosci.* (2011) 16:2812–902. doi: 10.2741/3887
60. Heyeraas KJ, Kim S, Raab WH, Byers MR, Liu M. Effect of electrical tooth stimulation on blood flow, interstitial fluid pressure and substance P and CGRP-immunoreactive nerve fibers in the low compliant cat dental pulp. *Microvasc Res.* (1994) 47:329–43. doi: 10.1006/mvre.1994.1026
61. Baluk P, Morikawa S, Haskell A, Mancuso M, McDonald DM. Abnormalities of basement membrane on blood vessels and endothelial sprouts in tumors. *Am J Pathol.* (2003) 163:1801–15. doi: 10.1016/S0002-9440(10)63540-7

62. Morikawa S, Baluk P, Kaidoh T, Haskell A, Jain RK, McDonald DM. Abnormalities in pericytes on blood vessels and endothelial sprouts in tumors. *Am J Pathol.* (2002) 160:985–1000. doi: 10.1016/S0002-9440(10)64920-6
63. Steitz SA, Speer MY, McKee MD, Liaw L, Almeida M, Yang H, et al. Osteopontin inhibits mineral deposition and promotes regression of ectopic calcification. *Am J Pathol.* (2002) 161:2035–46. doi: 10.1016/S0002-9440(10)64482-3
64. Bellahcene A, Castronovo V, Ogbureke KU, Fisher LW, Fedarko NS. Small integrin-binding ligand N-linked glycoproteins (SIBLINGs): multifunctional proteins in cancer. *Nat Rev Cancer.* (2008) 8:212–26. doi: 10.1038/nrc2345
65. Abd-Elmeguid A, Abdeldayem M, Kline LW, Moqbel R, Vliagoftis H, Yu DC. Osteocalcin expression in pulp inflammation. *J Endod.* (2013) 39:865–72. doi: 10.1016/j.joen.2012.12.035
66. Chen L, Jacquet R, Lowder E, Landis WJ. Refinement of collagen-mineral interaction: a possible role for osteocalcin in apatite crystal nucleation, growth and development. *Bone.* (2015) 71:7–16. doi: 10.1016/j.bone.2014.09.021
67. Nakashima K, Zhou X, Kunkel G, Zhang Z, Deng JM, Behringer RR, et al. The novel zinc finger-containing transcription factor osterix is required for osteoblast differentiation and bone formation. *Cell.* (2002) 108:17–29. doi: 10.1016/S0092-8674(01)00622-5
68. Zhao Y, Wang C, Li S, Song H, Wei F, Pan K, et al. Expression of osterix in mechanical stress-induced osteogenic differentiation of periodontal ligament cells *in vitro*. *Eur J Oral Sci.* (2008) 116:199–206. doi: 10.1111/j.1600-0722.2008.00533.x
69. Zeng J, Yang F, Zhang W, Gong Q, Du Y, Ling J. Association between dental pulp stones and calcifying nanoparticles. *Int J Nanomed.* (2011) 6:109–18. doi: 10.2147/IJN.S13267
70. Yang F, Zeng J, Zhang W, Sun X, Ling J. Evaluation of the interaction between calcifying nanoparticles and human dental pulp cells: a preliminary investigation. *Int J Nanomed.* (2010) 6:13–8. doi: 10.2147/IJN.S15064
71. Khan SR, Canales BK, Dominguez-Gutierrez PR. Randall's plaque and calcium oxalate stone formation: role for immunity and inflammation. *Nat Rev Nephrol.* (2021) 17:417–33. doi: 10.1038/s41581-020-00392-1
72. Blaser MC, Aikawa E. Roles and regulation of extracellular vesicles in cardiovascular mineral metabolism. *Front Cardiovasc Med.* (2018) 5:187. doi: 10.3389/fcvm.2018.00187
73. D'Souza A, Burch A, Dave KM, Sreeram A, Reynolds MJ, Dobbins DX, et al. Microvesicles transfer mitochondria and increase mitochondrial function in brain endothelial cells. *J Control Release.* (2021) 338:505–26. doi: 10.1016/j.jconrel.2021.08.038
74. Haney MJ, Zhao Y, Harrison EB, Mahajan V, Ahmed S, He Z, et al. Specific transfection of inflamed brain by macrophages: a new therapeutic strategy for neurodegenerative diseases. *PLoS ONE.* (2013) 8:e61852. doi: 10.1371/journal.pone.0061852
75. Kim J, Pannabecker TL. Two-compartment model of inner medullary vasculature supports dual modes of vasopressin-regulated inner medullary blood flow. *Am J Physiol Renal Physiol.* (2010) 299:F273–9. doi: 10.1152/ajprenal.00072.2010
76. Mocchegiani E, Basso A, Giacconi R, Piacenza F, Costarelli L, Pierpaoli S, et al. Diet (zinc)-gene interaction related to inflammatory/immune response in ageing: possible link with frailty syndrome? *Biogerontology.* (2010) 11:589–95. doi: 10.1007/s10522-010-9276-5
77. Frazzini V, Rockabrand E, Mocchegiani E, Sensi SL. Oxidative stress and brain aging: is zinc the link? *Biogerontology.* (2006) 7:307–14. doi: 10.1007/s10522-006-9045-7
78. Weidemann A, Johnson RS. Biology of HIF-1alpha. *Cell Death Differ.* (2008) 15:621–7. doi: 10.1038/cdd.2008.12
79. Kalucka J, Schley G, Georgescu A, Klanke B, Rossler S, Baumgartl J, et al. Kidney injury is independent of endothelial HIF-1alpha. *J Mol Med.* (2015) 93:891–904. doi: 10.1007/s00109-015-1264-4

Conflict of Interest: The authors declare that the research was conducted in the absence of any commercial or financial relationships that could be construed as a potential conflict of interest.

Publisher's Note: All claims expressed in this article are solely those of the authors and do not necessarily represent those of their affiliated organizations, or those of the publisher, the editors and the reviewers. Any product that may be evaluated in this article, or claim that may be made by its manufacturer, is not guaranteed or endorsed by the publisher.